

# Dynamics of the orientation of active and passive scalars in two-dimensional turbulence

G. Lapeyre,<sup>a)</sup> B. L. Hua, and P. Klein

*Laboratoire de Physique des Océans, IFREMER, BP 70, 29280 Plouzané, France and Laboratoire de Météorologie Dynamique, Ecole Normale Supérieure, 24 Rue Lhomond, 75230 Paris Cedex 05, France*

(Received 6 June 2000; accepted 21 September 2000)

The active nature of vorticity is investigated in order to understand its difference with a passive scalar. The direct cascade down to small scales is examined through both classical and new diagnostics (based on tracer gradient properties) in numerical simulations of freely decaying two-dimensional (2D) turbulence. During the transient evolution of turbulence, the passive scalar possesses a stronger cascade due to different alignment properties with the equilibrium orientations obtained in the adiabatic approximation by Lapeyre *et al.* [Phys. Fluids **11**, 3729 (1999)] and Klein *et al.* [Physica D **146**, 246 (2000)]. In strain-dominated regions, the passive scalar gradient aligns better with the equilibrium orientation than the vorticity gradient does, while the opposite is true in effective-rotation-dominated regions. A study of the kinematic alignment properties shows that this is due to structures with closed streamlines in the latter regions. However, in the final evolutionary stage of turbulence, both active and passive tracer gradients have identical orientations (i.e., there is a *perfect alignment* between the two gradients, all the more so when they are stronger). The effect of diffusion on the cascade is also studied. © 2001 American Institute of Physics. [DOI: 10.1063/1.1324705]

## I. POSITION OF THE PROBLEM

For the two-dimensional Euler equations, vorticity obeys the same equation as a passive scalar, in that it is conserved on Lagrangian trajectories. However, vorticity is linked in a *kinematic* sense to the velocity which advects it, since vorticity is the Laplacian of the stream function. The few studies concerned with this problem in two-dimensional (2D) turbulence<sup>1–3</sup> have pointed out differences and similarities between the two tracers. One striking similitude is that passive scalar and vorticity present similar shapes of filamentary structures.<sup>2,3</sup>

Several papers<sup>4–7</sup> have investigated the vorticity gradient dynamics and recent studies<sup>8,9</sup> have highlighted the importance of the dynamics of orientation of passive scalar gradient, taking into account the effect of the velocity and acceleration gradient tensors (as the latter has been shown to be essential for the dynamics<sup>7,10</sup>). Our aim is to use the concepts developed in these studies to revisit the problem of the nature, passive or active, of vorticity. Our analysis is based on the examination of the direct cascade of both tracers down to small scales. The manifestation of this cascade is the production of small scales, i.e., the production of *strong tracer gradients*. Analyzing these gradients for the two tracers should improve our knowledge of vorticity dynamics.

The present paper is an attempt to assess quantitatively the differences and similarities between the vorticity and passive scalar cascades using numerical simulations of 2D turbulence in free decay. The study uses several diagnostics related to the tracer cascades through the evolution of the turbulent field, both classical ones (spatial and spectral char-

acterizations of the cascades) but also original ones based on vorticity and passive scalar gradients, in particular their orientation properties. Moreover, the effect of diffusion on the cascade is also examined.

The first section of this paper is dedicated to a review of the different arguments (theoretical and observational) about what is known about vorticity and passive scalar cascades. Then, in Sec. II, we describe the numerical simulations used in this paper and the properties of their initial conditions. The third section is devoted to usual diagnostics of the tracer cascades. In Sec. IV, we examine the properties of the orientations of both tracers. This section reveals novel aspects of the cascades. Finally, we draw more general conclusions on the tracer cascades, summarizing the different aspects examined in this paper.

### A. Vorticity as an active tracer

There are several arguments for considering that vorticity should be dynamically active, i.e., should differ from a passive scalar. The first one is due to the fact that vorticity is kinematically related to the stream function and, thus, the enstrophy flux for a particular wave number in Fourier space has no local contribution. This behavior will occur if vorticity is a function of stream function ( $\omega = f(\psi)$ ): vorticity remains stationary, which is likely to occur for vortices. On the other hand, the passive scalar variance flux in spectral space has a contribution stemming from the interaction between the local wave numbers of, respectively, passive scalar and stream function.

Another, more restrictive, aspect of that kinematic relationship is the relationship in spectral space between vorticity and strain,<sup>5</sup>

<sup>a)</sup>Electronic mail: glapeyre@ifremer.fr

$$\hat{\sigma}_s(k) + i\hat{\sigma}_n(k) = i \frac{k}{k^*} \hat{\omega}(k),$$

where  $k = k_x + ik_y$  is the wave number in complex space and  $k^*$  its complex conjugate.  $\hat{\sigma}_s$ ,  $\hat{\sigma}_n$ , and  $\hat{\omega}$  are the Fourier components of, respectively, shear strain, normal strain, and vorticity (see Sec. IC for exact definitions).

This phase relationship between vorticity and strain was also noted by Ohkitani<sup>11</sup> as he found that these quantities are related in physical space by a conjugation relationship in two and three dimensions: the same integral transform (up to a minus sign) links the symmetric and antisymmetric part of the velocity gradient tensor. This conjugation relationship seems to prevent vorticity from cascading in three dimensions.<sup>12</sup>

One manifestation of these kinematic properties is that vorticity filaments are known to be unstable (the so-called Rayleigh<sup>13</sup> instability) and roll up in vortices. Thus vorticity structures have a feedback effect on the velocity field that advects them and can develop nontrivial behavior which differs from the passive scalar behavior.

Babiano *et al.*<sup>2</sup> and Ohkitani<sup>3</sup> have examined differences between vorticity and passive scalar in numerical simulations of forced turbulence in stationary state. They have observed that the scalar variance flux is greater than the enstrophy flux at the scales of vortices and this result should also hold for decaying turbulence. This difference was attributed to the role of vortices that tend to protect against the enstrophy cascade as confirmed by Babiano *et al.*<sup>2</sup> and McWilliams.<sup>14</sup> The enstrophy cascade is faster when the vortices are filtered than when the vortices are present. Thus the straining field produced by vortices is more efficient to transfer passive scalar variance than enstrophy to small scales.

## B. Vorticity as a passive tracer

One could object to these arguments that if the initial conditions of vorticity and passive scalar are identical, they remain identical through time evolution. However, the weakness of this argument is that it is a very particular solution.

The active nature of vorticity filaments can be questioned by the results of Dritschel *et al.*,<sup>15</sup> who showed that vorticity filaments do not develop the classical roll-up instability if they are exposed to external strain as small as 0.06 of the filament vorticity. The vortices of 2D turbulence can have a stabilization effect on the vorticity filaments as confirmed by Kevlahan and Farge.<sup>16</sup>

Concerning the conjugation relationship pointed out by Weiss<sup>5</sup> and Ohkitani,<sup>11</sup> its importance in two dimensions could be much more reduced than in three dimensions. In two dimensions, the cascade to small scales implies the production of vorticity *gradients*. If these gradients are uncorrelated with vorticity, it is not obvious that the conjugation relationship between strain and vorticity is able to impede the vorticity cascade, i.e., the production of vorticity gradients by straining processes.

Babiano *et al.*<sup>2</sup> noted in their numerical simulations the similar shapes of the small-scale structures of the vorticity and the passive scalar outside the coherent vortices. They

also observed that vorticity and passive scalar have much more similar spectra for structures containing a small amount of vorticity than for the entire flow. Thus it is tempting to state that the small-scale structures of vorticity outside the vortices should be passive and possess a similar cascade to the passive scalar one.

## C. Tracer dynamics

We need to know the properties of the tracer cascade in order to compare vorticity and passive scalar cascades. This cascade is related to the production of small scales, i.e., strong *tracer gradients*. Lapeyre *et al.*<sup>8</sup> and Klein *et al.*<sup>9</sup> have recently addressed the dynamics of tracer gradient formation. Let us summarize their basic results as they will be used in the present paper.

Consider a tracer  $q$  which is advected along Lagrangian trajectories. Its gradient verifies the equation

$$\frac{D\nabla q}{Dt} = -[\nabla\mathbf{u}]^*\nabla q,$$

where  $[\nabla\mathbf{u}]^*$  is the transpose of the velocity gradient tensor. This tensor can be decomposed into three parts: vorticity  $\omega$ , shear strain  $\sigma_s$ , and normal strain  $\sigma_n$ . It is more convenient to split the strain field into its norm and orientation and to decompose the passive scalar gradient  $\nabla q$  in the same way,

$$\begin{aligned}\sigma_n &= \partial_x u - \partial_y v, & \nabla q &= \rho(\cos\theta, \sin\theta), \\ \sigma_s &= \partial_x v + \partial_y u, & (\sigma_s, \sigma_n) &= \sigma(\cos 2\phi, \sin 2\phi), \\ \omega &= \partial_x v - \partial_y u & \text{with } \rho \geq 0 \text{ and } \sigma \geq 0.\end{aligned}$$

The key result pointed out by Lapeyre *et al.*<sup>8</sup> is that the equation of the relative orientation of the tracer gradient (which makes an angle  $\theta$  with the  $x$ -axis) with respect to the compressional strain axis (which makes an angle  $\pi/4 - \phi$  with the  $x$ -axis) characterizes the full tracer gradient dynamics,

$$\begin{aligned}\zeta &= 2(\theta + \phi), \\ \frac{D\zeta}{Dt} &= \omega + 2\frac{D\phi}{Dt} - \sigma \cos \zeta = \sigma(r - \cos \zeta).\end{aligned}\tag{1}$$

Lapeyre *et al.*<sup>8</sup> and Klein *et al.*<sup>9</sup> studied this equation, which is not closed in the sense that  $\sigma$ ,  $r$ , and  $\zeta$  are time dependent. Under the assumption that  $r$  is slowly varying (the so-called ‘‘adiabatic approximation’’), there are two dynamical regimes for the orientation  $\zeta$ , depending on the parameter  $r = (\omega + 2(D\phi/Dt))/\sigma$ . This parameter defines the competition between effective rotation effects [the sum of vorticity  $\omega$  and of the rotation of the strain axes  $2(D\phi/Dt)$ ] and straining effects. The first effect tends to rotate the gradient while the second effect tends to align it with the strain axes.

In regions of the flow where straining effects dominate ( $|r| < 1$ ), the orientation should tend to a stable fixed point of Eq. (1), i.e.,

$$\zeta = \zeta_- \equiv -\arccos r,$$

when making an adiabatic approximation.<sup>8</sup> Moreover, the tracer gradient norm  $\rho$  should grow exponentially in time. This regime corresponds to an intense cascade of tracer.

In the regime where effective rotation effects dominate ( $|r| > 1$ ), the tracer gradient should rotate but the rotation rate  $D\zeta/Dt$  depends on time. Thus the orientation of minimal rotation rate corresponds to the orientation along which the gradient spends most of its time. This orientation depends on  $r$  but also on the Lagrangian evolution of the rate of strain  $s = (1/\sigma^2)(D\sigma/Dt)$ . Thus, the orientation  $\zeta$  should be statistically close to the orientation of minimal rotation rate, i.e.,

$$\zeta = \alpha \equiv \arctan(s/r) + (1 - \text{sign}(r)) \frac{\pi}{2},$$

again when making an adiabatic approximation.<sup>9</sup> Moreover, the gradient norm  $\rho$  should evolve slowly, corresponding to a weak cascade.

These results were obtained by examining the equilibrium solutions of the orientation equation when  $r$  and  $s$  are slowly varying functions of time. They were validated for the strongest gradients in numerical simulations of two-dimensional turbulence<sup>8,9</sup> and confirm the important roles played by both the velocity gradient tensor (through  $\sigma$  and  $\omega$ ) and the acceleration gradient tensor (through  $D\phi/Dt$  and  $D\sigma/Dt$ ) as previously noted by Basdevant and Philipovitch<sup>17</sup> and Hua and Klein.<sup>7</sup> The orientation and gradient norm approaches quantitatively improve the representation of the tracer gradient dynamics with respect to previous studies.<sup>4,5</sup>

Thus, if the adiabatic approximation is valid, the tracer gradient orientation  $\zeta$  should align with these equilibrium orientations related to the flow topology. This is confirmed by numerical simulations, particularly for the largest gradients. This result is based only on the conservation of the tracer on Lagrangian trajectories, which is true for both vorticity and passive scalar and thus there is *a priori* no reason for a difference of their alignment properties.

#### D. Diffusion effects on tracer gradients

The effect of diffusion on the cascade properties is little documented. It is generally assumed that its role is to damp the norm of the tracer gradient. To our knowledge, only two papers examine its effect on the orientation of the gradient. Protas *et al.*<sup>6</sup> observed in their numerical simulations of 2D forced turbulence that when increasing the Reynolds number (by using hyperviscosity instead of Newtonian viscosity), the vorticity gradients align better with the compressional strain axis. On the other hand, Constantin *et al.*<sup>18</sup> develop qualitative results on the effect of diffusion, neglecting the effect of the cascade dynamics. Starting from the equation of advection-diffusion

$$\frac{Dq}{Dt} = \nu \Delta q,$$

we obtain the equation for the norm  $\rho$  and the orientation  $\theta$  of the tracer gradient  $\nabla q = \rho(\cos \theta, \sin \theta)$ ,

$$\begin{aligned} \frac{D\rho}{Dt} &= -\frac{\rho}{2} \sigma \sin \zeta + \frac{\nu}{\rho} \nabla q \cdot \nabla(\Delta q) \\ &= -\frac{\rho}{2} \sigma \sin \zeta + \nu \Delta \rho - \nu \rho |\nabla \theta|^2, \end{aligned}$$

$$\begin{aligned} \frac{D\theta}{Dt} &= \omega - \sigma \cos \zeta + \frac{\nu}{\rho^2} (\nabla q \times \nabla \Delta q) \cdot \mathbf{k} \\ &= \omega - \sigma \cos \zeta + 2\nu \Delta \theta + \frac{4\nu}{\rho} \nabla \theta \cdot \nabla \rho, \end{aligned}$$

with  $\mathbf{k}$  the unit vector normal to the plane of motion.

These equations involve the classical diffusion terms ( $\nu \Delta \rho$  and  $\nu \Delta \theta$ ) whose effects are to suppress spatial inhomogeneities. However, there are other terms with different effects on the gradient properties.

Let us examine their effects assuming that the other terms (classical diffusion, vorticity, and strain) are negligible. The equations reduce to

$$\frac{D\rho}{Dt} = -\nu \rho |\nabla \theta|^2, \quad (2)$$

$$\frac{D\theta}{Dt} = \frac{2\nu}{\rho} \nabla \theta \cdot \nabla \rho. \quad (3)$$

On the one hand, from Eq. (2), for large spatial variations of  $\theta$ , there is an exponential decay of the gradient norm  $\rho$ . Thus regions of large spatial variations of  $\theta$  should be regions of small gradients.<sup>18</sup> On the other hand, the larger the gradient norm  $\rho$  is, the smaller the diffusion effect on the orientation should be, because the diffusive term in Eq. (3) should be weak. Moreover, Constantin *et al.*<sup>18</sup> showed that this diffusive term is responsible for the spatial alignment of the tracer gradients with the direction of the largest gradients present in the field.

## II. INITIAL CONDITIONS AND THEIR CASCADE PROPERTIES

### A. Initial conditions

In order to explore the differences of passive and active tracer cascades, we have used numerical simulations of freely decaying two-dimensional turbulence. Vorticity is then a true Lagrangian invariant like the passive scalar, which is not the case in forced simulations. The code used here is a pseudo-spectral code detailed in Hua and Haidvogel<sup>19</sup> at a resolution of  $1024 \times 1024$ . The numerical diffusion is a Laplacian for both vorticity and passive scalar with the same coefficient of diffusion ( $\nu = 1.5 \times 10^{-5}$ ). The total kinetic energy is set to 1. This yields a Reynolds number of the order  $\text{Re} = UL/\nu \approx 4.2 \times 10^5$  (with  $L = 2\pi$ ).

The initial conditions correspond to the same spectra for vorticity and passive scalar but with random phases of their Fourier components. We have performed different simulations with different initial spectral slopes, and only two types of behavior, namely the dominance of either large or small scales, seem to matter as previously noted by Santangelo *et al.*<sup>20</sup>

The first set of simulations corresponds to large or intermediate scales. The simulation studied here will be initially

$$k \hat{\omega}_k \hat{\omega}_k^* = k \hat{c}_k \hat{c}_k^* = k \exp(-(k-10)^2), \quad (4)$$

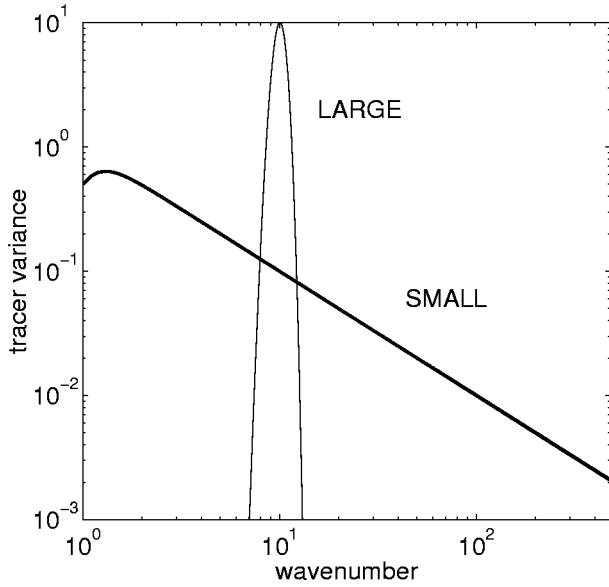


FIG. 1. Initial tracer spectra for simulations LARGE (solid curve) and SMALL (bold curve).

where  $\hat{x}_k$  corresponds to the Fourier component of  $x$  at wave number  $k$  and  $\hat{x}_k^*$  corresponds to its complex conjugate,  $\omega$  is the vorticity, and  $c$  the passive scalar.

This simulation corresponds to a peak at  $k=10$  in tracer spectra as displayed on Fig. 1. We call this simulation LARGE. It corresponds initially to structures with closed streamlines [see Fig. 2(a)] and it allows quasi-inviscid dynamics in the beginning of the simulation (because of the absence of small scales). This point will be shown below.

The second set corresponds to small-scale initial structures. For instance, we take

$$k \hat{\omega}_k \hat{\omega}_k^* = k \hat{c}_k \hat{c}_k^* = k^5 / (1 + k^6).$$

We call this simulation SMALL. Its spectrum displayed on Fig. 1 has a  $k^{-1}$  slope at small scales, typical of 2D turbulence. In physical space, only very small-scale structures are initially present [see Fig. 3(a)] and diffusion is expected to act through the entire range of evolution.

## B. Kinematic properties of the initial conditions

An analysis of the kinematic properties of the initial conditions of the vorticity field can be done to know *a priori* the initial configuration of the enstrophy cascade. There are no such initial cascade properties for the passive scalar as it is decorrelated with the velocity field by the phase randomization.

The first quantity that can be examined is the degree of nonlinearities of our initial conditions. We know that vorticity is conserved on a Lagrangian trajectory, i.e.,

$$\partial_t \omega + \mathbf{u} \cdot \nabla \omega = 0.$$

There can be a substantial depletion of nonlinearities whenever the vorticity advecting term  $\mathbf{u} \cdot \nabla \omega = J(\psi, \omega)$  is weak. A nondimensional measure of this weakness is the pseudocorrelation coefficient,

TABLE I. Quantities related to kinematic properties of initial conditions of the two simulations.  $C$  is the correlation between  $\mathbf{u}$  and  $\nabla \omega$ .  $R$  is the alignment coefficient of the vorticity gradient with orientation  $\alpha$  in effective-rotation-dominated regions.  $S$  is the alignment coefficient with orientation  $\zeta_-$  in strain-dominated regions and  $N$  is the alignment coefficient with  $\alpha$  also in strain-dominated regions.

	$C$	$R$	$S$	$N$
LARGE	-0.60	0.70	0.09	0.47
SMALL	0.00	0.24	0.03	0.16

$$C = 2 \frac{\langle |\mathbf{u} \cdot \nabla \omega| \rangle}{\sqrt{\langle \mathbf{u}^2 \rangle \langle |\nabla \omega|^2 \rangle}} - 1.$$

Because of the random initial conditions, the spatial average  $\langle \mathbf{u} \cdot \nabla \omega \rangle$  vanishes, motivating the need for absolute value.  $C = 1$  corresponds to a perfect correlation between the two vectors while  $C = -1$  corresponds to a perfect anticorrelation (i.e., a reduction of nonlinearities). If the two vector fields are decorrelated then  $C = 0$ .

The quantity  $C$  is displayed in Table I for the two initial spectra. The initial condition LARGE has depleted nonlinearities ( $C = -0.6$ ), while the initial condition SMALL does not possess such a depletion and vorticity seems decorrelated with stream function. The same quantity for passive scalar (replacing  $\nabla \omega$  by  $\nabla c$  in  $C$ ) yields 0 for all initial conditions.

The kinematic properties of the vorticity cascade can be examined using a method similar to Shtilman *et al.*,<sup>21</sup> who investigate the existence of a kinematic origin for the alignment of the vorticity vector with the strain axes in three-dimensional turbulent flows. In the same way, we can examine the kinematic properties of alignment with the equilibrium directions derived in Lapeyre *et al.*<sup>8</sup> and Klein *et al.*<sup>9</sup> and explained in Sec. IC. The question which is addressed is how the conjugation between vorticity and strain (as explained in Sec. IA) affects the alignment properties with the equilibrium orientations of the orientation dynamics. Actually this conjugation relationship is all the more able to halt the cascade as it links quantities (strain, vorticity) directly involved in the production of vorticity gradients.

A measure of the alignment properties is given by three quantities that express the alignment for strong gradients, in regions dominated by strain ( $|r| = |(\omega + 2D\phi/Dt)/\sigma| < 1$ ) and regions dominated by effective rotation ( $|r| > 1$ ). These quantities are

$$R = \frac{\langle |\nabla \omega|^2 \cos(\zeta_\omega - \alpha) \rangle}{\langle |\nabla \omega|^2 \rangle} \quad \text{in effective rotation regions,}$$

$$S = \frac{\langle |\nabla \omega|^2 \cos(\zeta_\omega - \zeta_-) \rangle}{\langle |\nabla \omega|^2 \rangle} \quad \text{in strain regions,}$$

$$N = \frac{\langle |\nabla \omega|^2 \cos(\zeta_\omega - \alpha) \rangle}{\langle |\nabla \omega|^2 \rangle} \quad \text{in strain regions.}$$

Here we define  $\zeta_\omega = 2(\theta_\omega + \phi)$ , where  $\nabla \omega = |\nabla \omega|(\cos \theta_\omega, \sin \theta_\omega)$  and  $\zeta_c$  is defined in the same way for the passive scalar field. The symbol  $\langle \rangle$  denotes a spatial av-

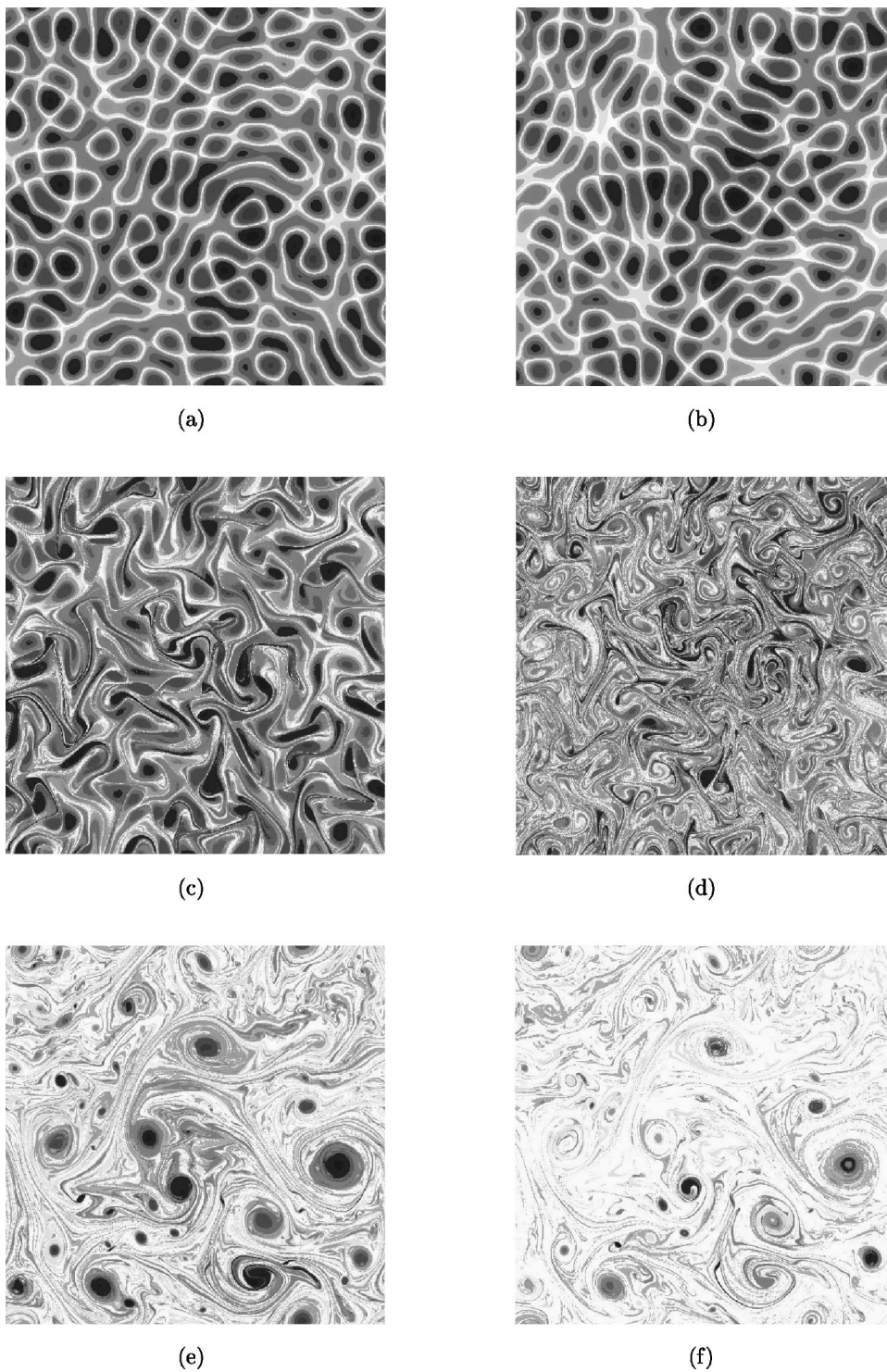


FIG. 2. (a), (c), (e) Vorticity field at time  $t=0, 1.02, 10.02$  for simulation LARGE. (b), (d), (e) Passive scalar field at the same times.

erage in regions of  $|r| < 1$  for  $S$  and  $N$  and in regions of  $|r| > 1$  for  $R$ . A value of 1 corresponds to perfect alignment with the orientation  $\zeta_-$  or  $\alpha$ . If the orientation is equipartitioned, we obtain 0 (but the reverse is not true). We have not examined the alignment with strain eigenvectors as in Protas *et al.*<sup>6</sup> because it is twice as weak as in our case.<sup>8,9</sup>

For the passive scalar field, we find that these quantities yield 0. The probability density functions (pdfs) of  $\zeta_c - \zeta_-$  and  $\zeta_c - \alpha$  are almost equipartitioned, confirming that there

is no alignment of passive scalar gradient with these equilibrium orientations (not shown).

From Table I, we note that initial conditions of simulation LARGE present a tendency to align with  $\alpha$  ( $R \approx 0.70$ ) in effective rotation regions (i.e., when  $|r| > 1$ ), whereas such a tendency is much more reduced for simulation SMALL ( $R \approx 0.24$ ). This has been confirmed by the alignment pdfs which exhibit a stronger peak for simulation LARGE than for simulation SMALL (not shown). Thus the effect of the

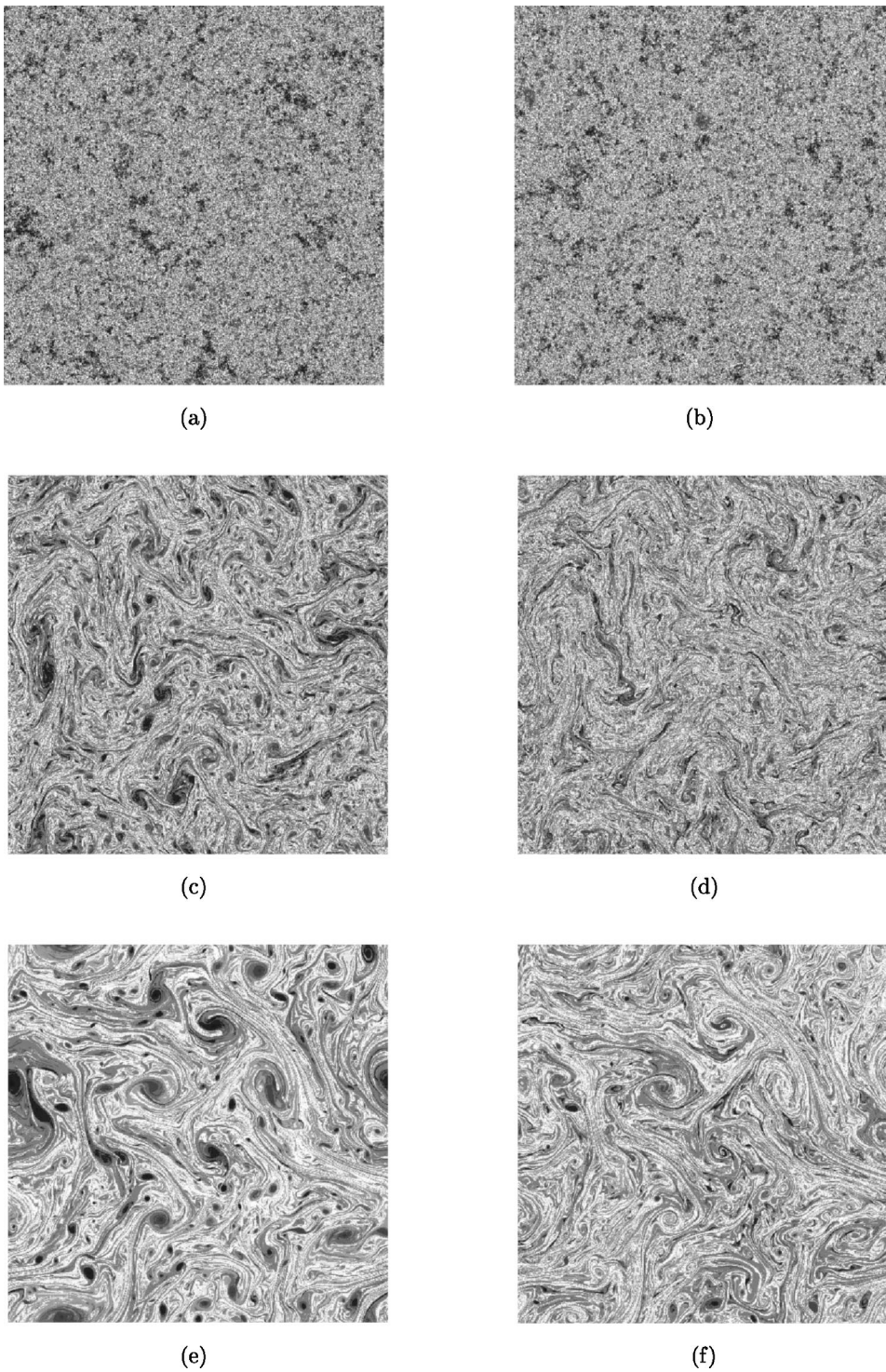


FIG. 3. (a), (c), (e) Vorticity field at time  $t=0, 1.14, 4.89$  for simulation SMALL. (b), (d), (e) Passive scalar field at the same times.

conjugation relationship between strain and vorticity depends on the types of structures present in the flow. If there are closed stream lines (as in simulation LARGE), the conjugation relationship aligns kinematically vorticity gradients with the equilibrium orientation of effective-rotation-dominated regions. We have checked that this result depends only on the geometry of the structures and not on their scales [i.e., taking a spectrum peak at  $k=100$  in Eq. (4) leads to similar values of  $R$ ]. Actually this alignment is associated with a weak cascade, i.e., a weak production of tracer gradients.<sup>9</sup> As a consequence, this kinematic alignment

linked to closed stream lines (i.e., vorticity patches) favors a weak cascade as previously observed by Babiano *et al.*<sup>2</sup> and McWilliams.<sup>14</sup> On the contrary, if there are no such structures present in the field, the conjugation relationship between strain and vorticity has no effect on the alignment.

In regions where strain dominates ( $|r| < 1$ ), we obtain small values of  $S$  for both initial conditions; thus there is no kinematic alignment with  $\zeta_-$  [also confirmed by the almost equipartitioned shape of the alignment p.d.f. (not shown)]. However, the kinematic alignment with  $\alpha$  seems to hold in regions dominated by strain but with a weaker amplitude

TABLE II. Different time scales related to the tracer cascade for the two simulations:  $\tau_{\text{adv}}$  is the time scale of the nondiffusive cascade (based on enstrophy).  $\tau_{\text{diff}}$  is the time scale of *diffusive* cascade as defined in Sec. II C.

	$\tau_{\text{adv}}$	$\tau_{\text{diff}}$	$\tau_{\text{diff}}/\tau_{\text{adv}}$
LARGE	0.100	0.441	4.65
SMALL	0.110	0.097	0.88

than in effective rotation regions, as  $N=0.47$  for simulation LARGE and  $N=0.16$  for simulation SMALL.

These kinematic results demonstrate that the conjugation relationship between vorticity and strain can only occur if the vorticity field possesses specific geometrical properties, such as the presence of closed streamlines (i.e., vorticity patches). Because of these structures, there is a kinematic alignment with the orientation  $\alpha$ , which is associated with a weak cascade.

### C. Inviscid and diffusive cascade time scales

We can define two time scales associated with the tracer cascades. The first time scale is related to the process of the nondiffusive cascade by stretching and folding of the scalar isolines. This time scale is

$$\tau_{\text{adv}} = \frac{1}{\sqrt{\langle \sigma^2 \rangle}},$$

where  $\sigma$  is the rate of strain and  $\langle \rangle$  is the spatial average. This is the usual enstrophy time scale as  $\langle \sigma^2 \rangle = \langle \omega^2 \rangle$  for 2D turbulence.

A second time scale intervenes if one takes into account the role of diffusion. Diffusion acts against strain on the spatial scale  $L_{\text{diff}} = (\nu \tau_{\text{adv}})^{1/2}$ . Consider a line element of width  $L_0$ . By stretching, its width decays in time as  $L(t) = L_0 \exp(-t/\tau_{\text{adv}})$ . Thus diffusion will be important at a time  $\tau_{\text{diff}}$  when  $L$  reaches the diffusive length scale  $L_{\text{diff}}$ ,

$$\tau_{\text{diff}} = \tau_{\text{adv}} \log \sqrt{\frac{L_0^2}{\nu \tau_{\text{adv}}}}.$$

Here  $L_0$  can be set by the typical wavelength of the vorticity gradient, for instance,

$$L_0^{-2} = \frac{\langle |\nabla \Delta \omega| \rangle}{\langle |\nabla \omega| \rangle}.$$

These time scales, as well as the ratio  $\tau_{\text{diff}}/\tau_{\text{adv}}$ , can be computed for the initial conditions (Table II). Simulation LARGE has a typical inviscid cascade time scale which is much shorter than the diffusive cascade time scale ( $\tau_{\text{diff}} = 4.65 \tau_{\text{adv}}$ ) while these two time scales are comparable for simulation SMALL. This means that diffusion is likely to be negligible in the tracer cascade processes for simulation LARGE for a time  $t < \tau_{\text{diff}}$ . For simulation SMALL, diffusion will be important *ab initio*.

## III. PHYSICAL AND SPECTRAL CHARACTERIZATION OF THE CASCADES

### A. Evolution in physical space

It is interesting to examine the time evolution of the vorticity and passive scalar fields to assess their differences. The evolution of the vorticity field is well described in the literature.<sup>20,22,23</sup>

Let us consider first simulation LARGE. Initially, the vorticity field and the passive scalar field are decorrelated in space but present the same types of structures [Figs. 2(a) and 2(b)]. In the very early stage of evolution ( $t \approx 3 \tau_{\text{adv}}$ ), the vortices do distort the passive scalar field but remain quasistationary themselves, a result also present in Holloway and Kristmannsson.<sup>1</sup> Later on, the vortices begin to interact with each other, a process which creates filaments of vorticity while shearing the weakest vortices [Fig. 2(c)]. During the same time, the passive scalar reaches the diffusive length scale and becomes homogenized very rapidly both outside and inside vortices [Fig. 2(d)]. In the final evolutionary stage of turbulence, the vorticity field displays the presence of coherent vortices and vorticity filaments [Fig. 2(e)]. The passive scalar field displays the same kind of geometry [Fig. 2(f)]: homogenized regions inside vortices and filaments outside. As vortices are present from the start, the vorticity field is more homogenized inside the vortices than the scalar field which often forms spirals. This simulation shows that the process of production of small scales is faster for the scalar field than for the vorticity field. The initial presence of the vortices seems to inhibit the cascade of vorticity to small scales.

The evolution of simulation SMALL is different. Initially, there are very small scale structures [Figs. 3(a) and 3(b)]. These structures interact by straining and diffusive processes and vortices emerge slowly [Fig. 3(c)]. The tracer field evolves in the same way [Fig. 3(d)]. In the final evolutionary stage of turbulence, larger vortices develop [Fig. 3(e)] and shear the passive scalar field [Fig. 3(f)] as also found in simulation LARGE.

### B. Spectral evolution

As the total tracer variance constantly decreases because of dissipation, the tracer spectra are nondimensionalized such that a value of 1 is obtained for  $k=20$ . This procedure allows us to examine the evolution of the slope of the spectra at large scales and at small scales.

Simulation LARGE has initially a spectrum peaked at  $k=10$  for both vorticity and passive scalar. As time evolves, the enstrophy spectrum spreads more and more to small scales as well as to large scales [Fig. 4(a)]. When the enstrophy spectrum fills the whole wave number space, it exhibits a spectral slope steeper than  $-1$  (around  $-1.4$ ) at the intermediate scales  $7 < k < 100$  (curves E and F). Moreover, we observe the accumulation of enstrophy at large scales, because of the inverse energy cascade. The passive scalar spectrum has a faster development [Fig. 4(b)]. The passive scalar slope is shallower (around  $-0.9$ ) at intermediate scales in the final evolutionary stage of turbulence [see also Fig. 4(e)].

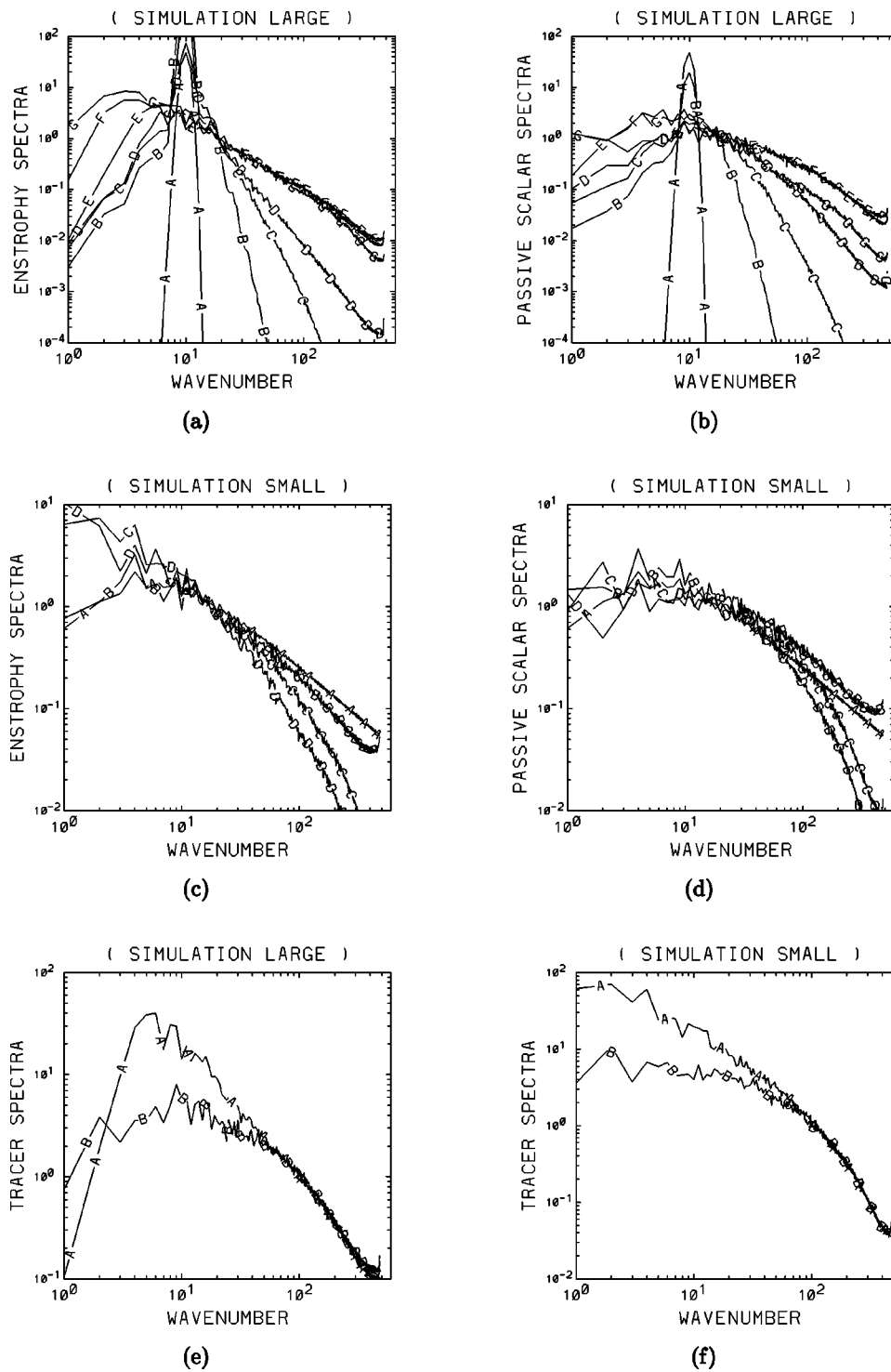


FIG. 4. (a), (c) Enstrophy spectra. (b), (d) Passive scalar spectra. Simulation LARGE (a), (b) at  $t=0, 0.06, 0.18, 0.46, 1.86, 4.74, 8.1$  (A)–(G). Simulation SMALL (c), (d) at  $t=0, 0.45, 5.79, 10.5$  (A)–(D). (e), (f): curve A, vorticity spectrum; curve B, passive scalar spectrum. (e) Simulation LARGE at  $t=1.86$ . (f) Simulation SMALL at  $t=4.89$ .

But we observe a steepening of the slope at later time (curve G), due to the dissipation that permanently removes enstrophy and scalar variance at small scales.

Initially, for simulation SMALL, the tracer spectra have a power law  $k^{-1}$  at small and intermediate scales [Figs. 4(c) and 4(d)]. This power law is modified by dissipation at small scales and the spectra become steeper and steeper. At large scales, we observe the accumulation of enstrophy while the passive scalar spectrum seems stationary.

A comparison of both tracers in the final evolutionary stage of turbulence, before dissipation begins to erode the

spectra completely, shows that vorticity and passive scalar have identical spectra at small scales [Figs. 4(e) and 4(f)]. At intermediate scales, passive scalar spectra are shallower than vorticity spectra. At large scales, we observe (at later times) the accumulation of enstrophy which is absent for passive scalar. The overlap of the two tracer spectra at small scales could imply an identical nature of the cascade for both tracers, even if there were differences during the transient development of the spectra. The major difference appears at large and intermediate scales where enstrophy seems to move toward large scales: because of the inverse energy cascade and

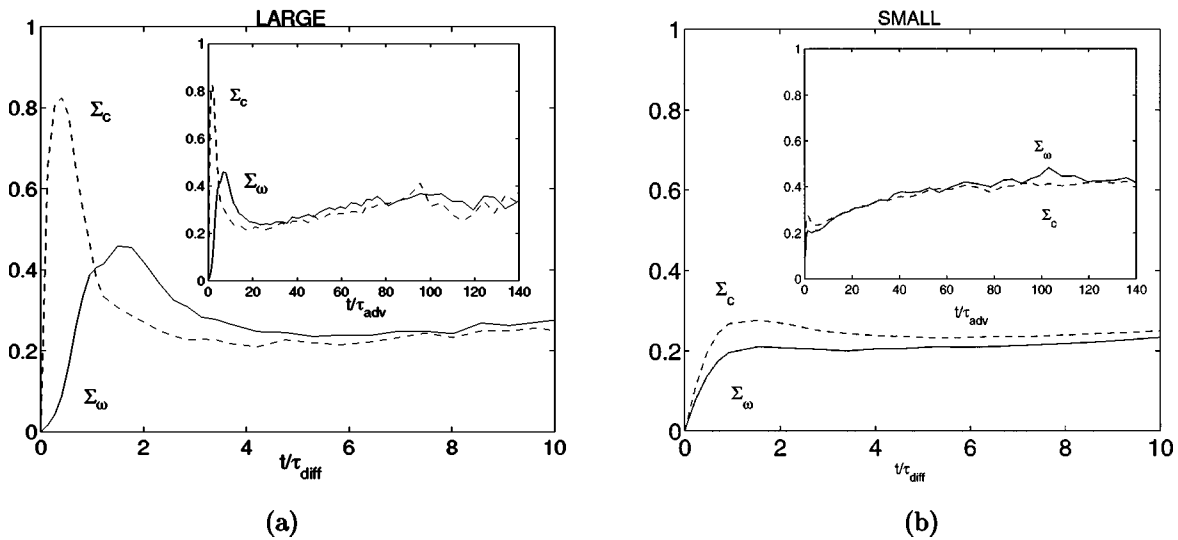


FIG. 5. Time evolution of the cascade efficiencies  $\Sigma_\omega$  and  $\Sigma_c$  for simulations LARGЕ (a) and SMALL (b); the abscissa is  $t/\tau_{\text{diff}}$  in the main figure,  $t/\tau_{\text{adv}}$  in the inset. Solid curves: vorticity efficiency  $\Sigma_\omega$ . Dashed curves: passive scalar efficiency  $\Sigma_c$ .

the accumulation of vorticity into vortices, an amount of enstrophy is cascading to large scales, which produces a steeper spectrum for vorticity than for passive scalar, since such a behavior is absent for the latter.

### C. Cascade efficiency

A widely used diagnostic of the cascade is given by the efficiency parameters (or two-dimensional skewness<sup>23</sup>)  $\Sigma_\omega$  and  $\Sigma_c$ . This quantity is related to the inviscid equation for the tracer gradient, for instance vorticity gradient,

$$\frac{D|\nabla\omega|^2}{Dt} = -|\nabla\omega|^2 \sigma \sin \zeta_\omega.$$

The efficiency parameter allows us to quantify whether the cascade has reached its maximal gradient growth rate,

$$\Sigma_\omega = \frac{-\langle |\nabla\omega|^2 \sigma \sin \zeta_\omega \rangle}{\langle |\nabla\omega|^2 \rangle \langle \sigma^2 \rangle^{1/2}} = \frac{1}{\langle |\nabla\omega|^2 \rangle} \left\langle \frac{D|\nabla\omega|^2}{D(t/\tau_{\text{adv}})} \right\rangle.$$

We define  $\Sigma_c$  in the same way, but replacing  $|\nabla\omega|$  by  $|\nabla c|$  and  $\zeta_\omega$  by  $\zeta_c$ . Note that  $\sin \zeta_\omega = -1$  corresponds to the alignment of the vorticity gradient with the compressional strain axis, i.e., the eigenvector of the strain rate tensor responsible for tracer gradient growth.

These efficiency parameters are displayed in Figs. 5(a) and 5(b) for the two simulations. Because of the random phase initialization,  $\Sigma = 0$  initially. From the start,  $\Sigma$  becomes and remains positive, which corresponds to the production of tracer gradients (note that its definition does *not* imply positiveness).

For both simulations, we observe that the passive scalar efficiency increases more strongly than the vorticity efficiency. An explanation could be the conjugation relationship between vorticity and strain. This seems confirmed by the larger ratio  $\Sigma_c/\Sigma_\omega$  for simulation LARGЕ than for SMALL (1.80 against 1.31) since simulation LARGЕ has initially

stronger kinematic properties. Moreover, in the final evolutionary stage of turbulence, the quantities  $\Sigma_c$  and  $\Sigma_\omega$  reach a mean plateau around 0.4.

Initially, the efficiency parameter is much smaller in simulation SMALL than in simulation LARGЕ. A possible explanation is the important initial effect of diffusion in simulation SMALL, which could decrease the alignment with the strain axes. This is confirmed by the local maximum of the efficiency parameter occurring at time  $t \approx \tau_{\text{diff}}$  for both simulations. This result could be consistent with the result of Protas *et al.*<sup>6</sup> which indicates a better alignment with the compressional strain axis when the Reynolds number increases.

## IV. ALIGNMENT PROPERTIES OF TRACER GRADIENTS

Another aspect of the tracer cascade concerns the alignment of tracer isolines with the flow topology and the alignment of the two tracers with each other. Actually in the adiabatic approximation and in a nondiffusive situation, the flow topology forces any tracer gradient to align with equilibrium orientations.<sup>8,9</sup> Some qualitative results<sup>2,3</sup> observe similar tracer isolines (i.e., a tendency for an alignment between the two tracer gradients). Our numerical simulations can be used to confirm quantitatively this fact and also to investigate the role of diffusion on the orientation dynamics.

### A. Diffusion effect on alignment

First, let us examine the effect of diffusion on the orientation of tracer gradient in order to explain the time evolution of our diagnostics. The equation for the vorticity gradient orientation taking into account Newtonian diffusion is

$$\frac{D2\theta_\omega}{Dt} = \omega - \sigma \cos \zeta_\omega + \mathcal{D}_\omega, \quad (5)$$

with  $\mathcal{D}_\omega$  the diffusive term,

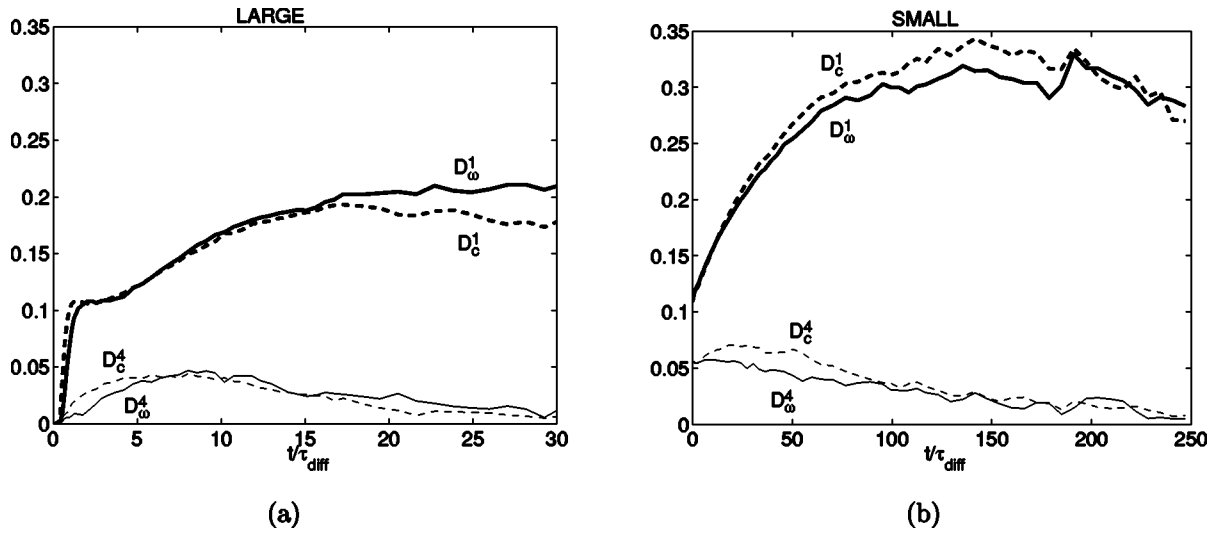


FIG. 6. Evolution of the ratio between contributions of diffusion and advective dynamics to the alignment Eq. (5) as a function of  $t/\tau_{\text{diff}}$  for simulations LARGE (a) and SMALL (b). Solid curves:  $D_\omega^1$  (bold),  $D_\omega^4$  (light). Dashed curves:  $D_c^1$  (bold),  $D_c^4$  (light).

$$\mathcal{D}_\omega = \frac{\nu}{|\nabla \omega|^2} (\nabla \omega \times \nabla (\Delta \omega)) \cdot \mathbf{k},$$

where  $\mathbf{k}$  is the unit vertical vector.

We can compute the ratio between diffusion effects and dynamical effects in Eq. (5) with a tracer gradient weighting,

$$D_\omega^n = \sqrt{\frac{\langle |\nabla \omega|^n \mathcal{D}_\omega^2 \rangle}{\langle |\nabla \omega|^n (\omega^2 + \sigma^2) \rangle}}$$

is defined for vorticity. We define the same quantity  $D_c^n$  for passive scalar by replacing  $\mathcal{D}_\omega$  by  $\mathcal{D}_c$  and  $\nabla \omega$  by  $\nabla c$ . The exponent  $n$  is varied to assess the weight due to the strongest gradient values. Thus increasing  $n$  is similar to restricting the averaging to regions of stronger and stronger gradients.

Figures 6(a) and 6(b) display these quantities for the two simulations. We have plotted only the cases  $n=1$  and  $n=4$  as there is a monotone decrease of the ratios when  $n$  increases (not shown). We can see that the effect of the diffusion decreases when we consider larger gradients as  $D_\omega^n$  and  $D_c^n$  decreases when  $n$  increases, confirming the prediction of Constantin *et al.*<sup>18</sup> stated in Sec. ID. For the largest gradients, the ratio between diffusion effects and dynamical effects is less than 5%. This confirms that we can neglect diffusion as was done in our previous theoretical studies.<sup>8,9</sup>

Now let us examine simulation LARGE [Fig. 6(a)]. Initially, the diffusion is negligible ( $D_\omega^n$  and  $D_c^n$  are of the order of  $10^{-5}$ ). Around  $t \approx \tau_{\text{diff}}$ , a sudden rise occurs, followed by a slower increase and then by a slow decay. The growth of  $D_\omega^n$  and  $D_c^n$  can be interpreted as the production of small scales which enhances the diffusion terms. The decay could be explained by the mechanism of Constantin *et al.*<sup>18</sup> as diffusion tends to smooth the spatial field of the orientation (by affecting both tracer gradient norm and orientation), its effect becomes smaller (there are less and less spatial inhomogeneities). Diffusion affects the passive scalar gradient orientation before the vorticity gradient orientation but the difference is reduced for the strongest gradients. This can be

explained by the more rapid cascade, i.e., production of small-scale inhomogeneities, for passive scalar than vorticity as we have seen in previous section.

The results of simulation SMALL [Fig. 6(b)] are similar to simulation LARGE but diffusion is larger in this simulation since there are initially more spatial inhomogeneities.

We have also examined the effect of diffusion on strain-dominated and effective-rotation-dominated regions. Diffusion has less influence in effective-rotation regions than in strain-dominated regions with a difference of 10% (not shown). In strain-dominated regions, a strong cascade, i.e., a production of small scales (and small-scale inhomogeneities) is expected and the effect of diffusion should be important there.

## B. Dynamical alignment with flow topology

As shown by Lapeyre *et al.*<sup>8</sup> and Klein *et al.*<sup>9</sup> in the adiabatic approximation, there are two different regions for the dynamics of tracer gradient, namely when strain dominates ( $|r| \equiv |(\omega + 2D\phi/Dt)/\sigma| \leq 1$ ) and when effective-rotation dominates ( $|r| > 1$ ). For the former regime, the orientation variable  $\zeta$  should tend to  $\zeta_-$ , while for the latter regime, the orientation should rotate with time but remains statistically close to  $\alpha$ .

We can examine if these alignments occur and how vorticity and passive scalar gradients differ. For this purpose, we define spatial averages of the cosine between  $\zeta$  and the equilibrium orientation ( $\zeta_-$  in strain regions,  $\alpha$  in effective rotation regions). We weight these spatial averages by the same exponent on both tracer gradient norms to compare regions that should be similar for the two gradients. These diagnostics are

$$S_\omega^n = \frac{\langle |\nabla \omega|^n |\nabla c|^n \cos(\zeta_\omega - \zeta_-) \rangle}{\langle |\nabla \omega|^n |\nabla c|^n \rangle} \quad \text{in strain regions,}$$

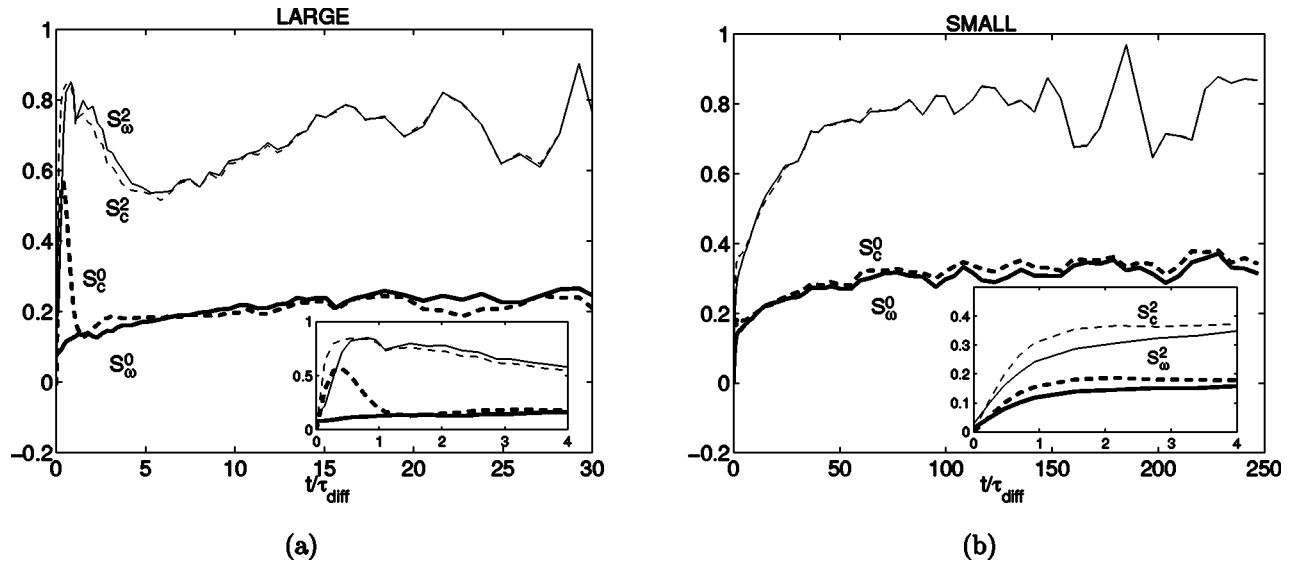


FIG. 7. Evolution of the dynamical alignment in strain-dominated regions as a function of  $t/\tau_{\text{diff}}$  for simulations LARGE (a) and SMALL (b). In inset, zoom of initial evolution. Solid curves:  $S_{\omega}^0$  (bold),  $S_{\omega}^2$  (light). Dashed curves:  $S_c^0$  (bold),  $S_c^2$  (light).

$$R_{\omega}^n = \frac{\langle |\nabla \omega|^n |\nabla c|^n \cos(\zeta_{\omega} - \alpha) \rangle}{\langle |\nabla \omega|^n |\nabla c|^n \rangle}$$

in effective rotation regions.

At each time, spatial averaging  $\langle \rangle$  is performed in strain-dominated regions ( $|r| < 1$ ) for  $S_{\omega}^n$ , and in effective-rotation-dominated regions ( $|r| > 1$ ) for  $R_{\omega}^n$ . The statistics are thus done for regions that change constantly in time. The diagnostics has been normalized: if  $\zeta - \zeta_{-}$  (respectively  $\zeta - \alpha$ ) is equipartitioned, then  $S_{\omega}^n = 0$  (resp.  $R_{\omega}^n = 0$ ). On the other hand, a value of 1 corresponds to perfect alignment. We define  $S_c^n$  and  $R_c^n$  in the same way for the passive scalar (i.e., we replace  $\zeta_{\omega}$  by  $\zeta_c$  in each formula).  $S$  stands for strain-dominated regions and  $R$  stands for effective-rotation-dominated regions.

### 1. Strain-dominated regions

Let us consider first the strain-dominated regions. In these regions, the tracer gradient is expected to align with the orientation  $\zeta_{-}$ , the stable fixed point of Eq. (1), if the adiabatic approximation is valid.

For simulation LARGE [Fig. 7(a)], there is no initial alignment of both tracer gradients with this orientation (as shown in Sec. II B):  $S_{\omega}^n = S_c^n \approx 0$ . As time evolves, both tracer gradients tend to align strongly with the equilibrium direction  $\zeta_{-}$ . Actually the alignment increases monotonously with  $n$  (not shown), which means that the larger the tracer gradients are, the better they align with  $\zeta_{-}$  while there is not such a specific trend for the weakest gradients.

At time  $t \approx \tau_{\text{diff}}$ , we observe a decrease in alignment. This decrease is related to diffusion which becomes important at that time, as seen in Sec. IV A. However,  $S_{\omega}^n$  and  $S_c^n$  increase once again (at time  $t \approx 6\tau_{\text{diff}}$  for  $n=2$ ) to reach a mean plateau, different from perfect alignment. We can note that there are substantial oscillations around this mean pla-

teau. This is due to the weighting by the tracer gradient norm which takes into account only a small part of the total field.

Now we can compare the evolution of the alignment of the vorticity gradient (solid curve on the figure) and the passive scalar gradient (dashed curve) with  $\zeta_{-}$ . For early time ( $t < \tau_{\text{diff}}$ ), the passive scalar gradient aligns better with the equilibrium orientation  $\zeta_{-}$  than the vorticity gradient does. This means that the direct cascade is more efficient for passive scalar than for vorticity. At time  $t \approx \tau_{\text{diff}}$ , we observe that  $S_{\omega}^n$  and  $S_c^n$  overlap for  $n=2$ . This is also true for  $n \geq 3$  (not shown) and it indicates that tracer gradients align with each other (this will be examined further). Because diffusion is stronger for the passive scalar gradient orientation,  $S_c^2$  decreases more strongly than  $S_{\omega}^2$ . Finally, the two curves overlap again at  $t \approx 7\tau_{\text{diff}}$ .

For simulation SMALL [Fig. 7(b)], we observe similar behaviors, except that the initial alignment increase is much more reduced as diffusion acts *ab initio*. The saturation of alignment occurs also at  $t \approx \tau_{\text{diff}}$  as for simulation LARGE and we can be confident that the saturation is due to diffusion.

### 2. Effective-rotation-dominated regions

We can consider the dynamical alignment properties in effective-rotation-dominated regions. The tracer gradient is expected to rotate at a nonconstant rotation rate and should lie statistically close to the equilibrium orientation  $\alpha$ , if the adiabatic approximation is valid.

Figure 8(a) displays  $R_{\omega}^n$  and  $R_c^n$  for  $n=0,2$  for simulation LARGE [actually we have checked that there is a monotone increase of  $R$  with  $n$  (not shown)]. Initially vorticity gradients display a tendency to align with the orientation given by  $\alpha$  ( $R_{\omega}^0 = 0.49$  and  $R_{\omega}^2 = 0.70$ ) whereas there is no such an alignment for passive scalar ( $R_c^n \approx 0$ ).  $R_c^n$  strongly increases until it reaches the same value as  $R_{\omega}^n$  at  $t \approx 0.5\tau_{\text{diff}}$ . For  $n=2$ , the two curves overlap during a time  $\tau_{\text{diff}}$  and then  $R_c^n$

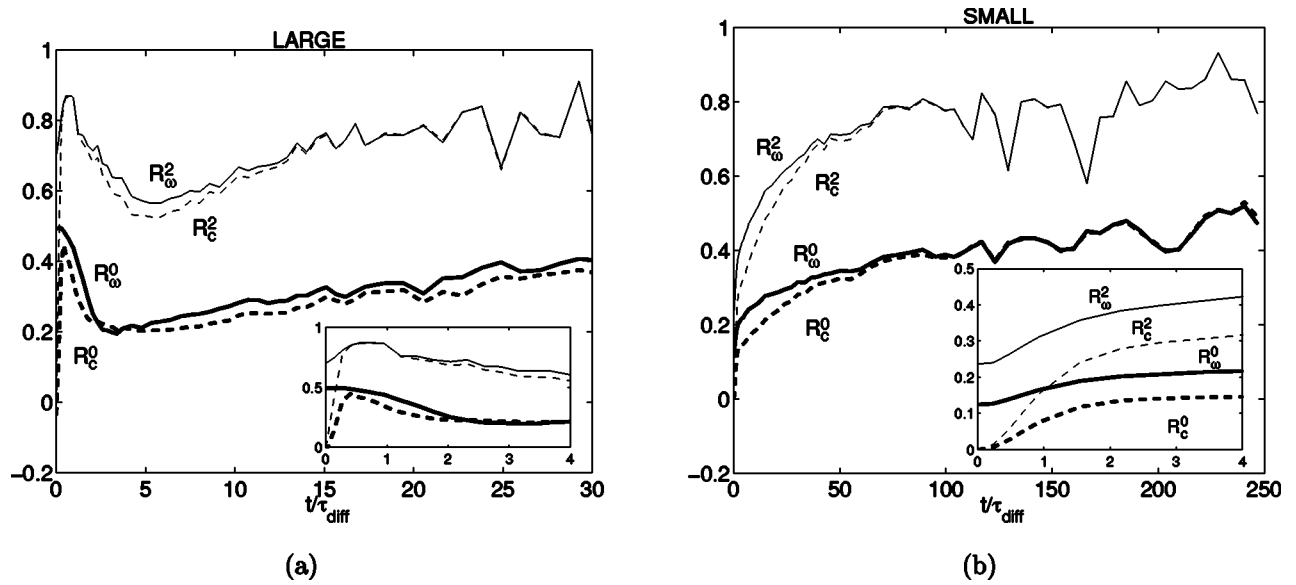


FIG. 8. Evolution of the dynamical alignment in effective-rotation-dominated regions as a function of  $t/\tau_{\text{diff}}$  for simulations LARGE (a) and SMALL (b). In inset, zoom of initial evolution. Solid curves:  $R_\omega^n$  (bold),  $R_\omega^2$  (light). Dashed curves:  $R_c^n$  (bold),  $R_c^2$  (light).

has a larger decrease than  $R_\omega^n$ . Contrary to what is found for strain-dominated regions, the alignment is always better (if not equal) for the vorticity gradients than for the passive scalar gradients. After this transient phase,  $R_c^n$  and  $R_\omega^n$  overlap again (at  $t \approx 13\tau_{\text{diff}}$  for  $n=2$ ) to reach a mean plateau with substantial oscillations as was also found previously in strain-dominated regions. When comparing Figs. 7(a) and 8(a), the final overlap of  $S_c^n$  and  $S_\omega^n$  occurs more rapidly in strain-dominated regions than the final overlap of  $R_c^n$  and  $R_\omega^n$  in effective-rotation-dominated regions. This can be explained by the different dynamics of the two regions: in strain regions, the orientation should tend to the equilibrium orientation  $\zeta_-$  whereas in effective rotation regions, the orientation should be rotating and only statistically close to another equilibrium orientation  $\alpha$ . This implies a faster process of alignment with the equilibrium orientation in strain-dominated regions than in effective-rotation-dominated regions.

For simulation SMALL [Fig. 8(b)], the initial phase of alignment increase is absent for both  $R_\omega^n$  and  $R_c^n$  because diffusion is present initially. It can be compared with simulation LARGE after diffusion has become efficient [i.e., after  $t > 5\tau_{\text{diff}}$  on Fig. 8(a)].

We can conclude that the alignment of the vorticity gradient with the equilibrium orientation  $\alpha$  has both a kinematic origin (the presence of spatial large-scale structures with closed streamlines) and a dynamical origin (dynamics of the vorticity gradient orientation). In the transient phase of turbulence, the kinematics improve the alignment of vorticity gradient with the equilibrium orientation more so than the alignment of passive scalar gradient. Despite this kinematic effect, passive scalar gradients and vorticity gradients have similar alignment properties with  $\alpha$  in the final evolutionary stage of turbulence.

### C. Alignment between passive and active scalar gradients

Motivated by the overlap of  $S_c^n$  and  $S_\omega^n$  on the one hand and  $R_c^n$  and  $R_\omega^n$  on the other hand, as well as the observations<sup>2,3</sup> of similar tracer isolines, we can define a quantity  $A_n$  to examine the alignment between vorticity gradients and passive scalar gradients,

$$A_n = \frac{\langle |\nabla \omega|^n |\nabla c|^n \cos(\zeta_\omega - \zeta_c) \rangle}{\langle |\nabla \omega|^n |\nabla c|^n \rangle}.$$

As for  $S_\omega^n$  and  $R_\omega^n$ , there is a symmetrical weight on both tracer gradients which allows us to compare regions where both gradients are expected to have a similar cascade. Moreover, gradient weighting increases with  $n$ .

As could be expected from the results on dynamical alignment, simulation LARGE displays three stages of evolution [Fig. 9(a)]. Initially, the two gradients are decorrelated because of the random phase initialization, so  $A_n = 0$ . There is a rapid increase of  $A_n$ , reaching a value close to 1 for  $n \geq 2$  at  $t \approx \tau_{\text{diff}}$ . The alignment improves when increasing  $n$ . This confirms that the direct cascade proceeds in the same way by aligning the two gradients, especially the strongest ones. After  $t \approx \tau_{\text{diff}}$ , diffusion becomes important and  $A_n$  decreases strongly. This lasts until  $t \approx 5\tau_{\text{diff}}$ . After this time, we observe an increase of  $A_n$  which tends to 1 (i.e., *perfect alignment* of the two gradients) for  $n \geq 2$ . For  $n=0$ , the simulation was not carried long enough to examine the convergence. Nevertheless, these results indicate that *the largest gradients of vorticity and passive scalar tend to align with each other*. We can suspect that this is due to both advective dynamics and diffusion: on the one hand, the dynamics of the tracer gradient tends to align tracer gradient with equilibrium orientations related to the flow topology. On the other hand, diffusion tends to reduce the gradients

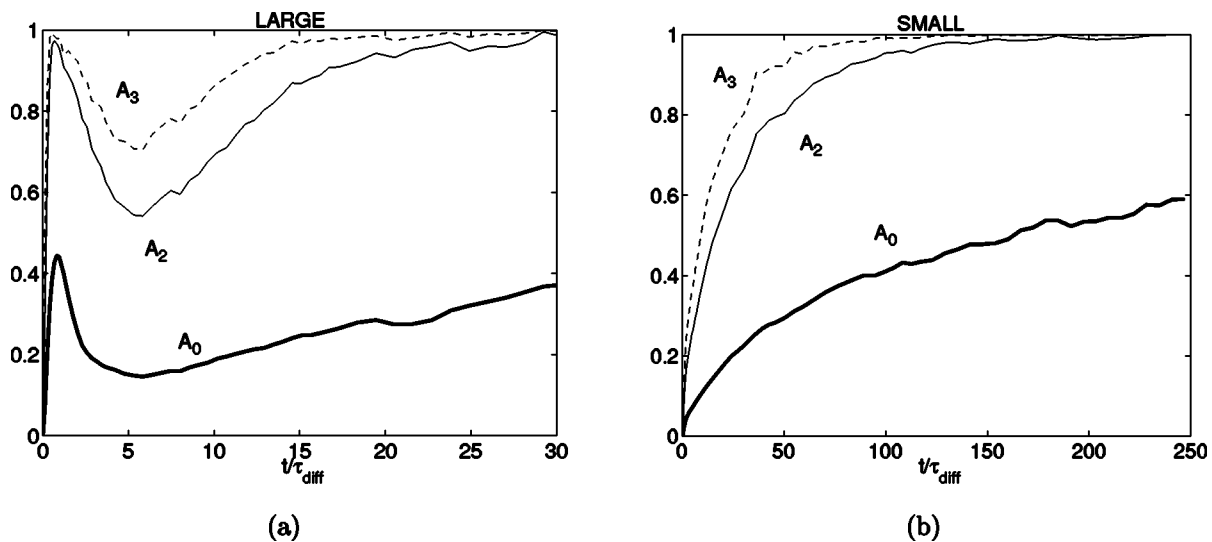


FIG. 9. Evolution of the orientation between the two gradients  $A_n$  as a function of  $t/\tau_{diff}$  for simulation LARGE (a) and SMALL (b). Bold curve:  $n=0$ . Solid curve:  $n=2$ . Dashed curve:  $n=3$ .

which are not aligned with these equilibrium orientations. Another aspect of diffusion is to align spatially tracer gradients with the direction of the largest gradients,<sup>18</sup> thus amplifying the alignment with the equilibrium orientations (as this latter mechanism is amplified for the strongest gradients). Thus, these effects contribute to a continuously growing alignment between the two tracer gradients. However, we have to put a *caveat* on this argument. Why don't we observe also a perfect alignment with the equilibrium orientations  $\zeta_-$  and  $\alpha$ ? A tentative answer is that  $\zeta_-$  and  $\alpha$  are only estimates of the real orientations given by the flow topology. Actually they are equilibrium estimates in the adiabatic approximation ( $r$  and  $s$  slowly varying in time) of these orientations.

For simulation SMALL [Fig. 9(b)], we observe only a slow increase of  $A_n$  like the final phase of simulation LARGE. This is due to diffusion which acts through the entire evolution. But we can see that there is also a perfect alignment for the strongest gradients in this case as in the preceding case.

## V. SUMMARY AND CONCLUSION

We have examined and compared the cascades of a passive scalar and vorticity in numerical simulations of freely decaying 2D turbulence. The two tracer fields have been initialized with identical spectra but with different phases, for two limiting (large- and small-scale) cases. Dissipative effects are treated identically for both active and passive tracers. The cascade dynamics is studied through the production of tracer gradients, and, more specifically, the tendency for alignment of those gradients with equilibrium directions<sup>8,9</sup> obtained in the adiabatic approximation.

The kinematic properties of the initial conditions reveal that the conjugation relationship between vorticity and strain slows down the cascade dynamics whenever structures with closed streamlines are present. This effect only operates for simulation LARGE, where a substantial alignment of vorticity gradients with the flow topology is observed in regions

dominated by effective rotation (i.e., the sum of vorticity and strain axes rotation rate). On the other hand, for simulation SMALL, diffusion effects are likely to be important *ab initio*, as indicated by an estimate of the inviscid and diffusive cascade time scales.

During the first transient phase of evolution, there is a stronger cascade for passive scalar than for vorticity. The passive scalar develops small scales very rapidly, being sheared by vortices (which remain quasistationary for simulation LARGE). This has been observed in both physical space and Fourier space. In strain-dominated regions, the passive scalar gradient aligns better than the vorticity gradient with the equilibrium orientation  $\zeta_-$  related to the flow topology. On the other hand, in effective-rotation-dominated regions, the vorticity gradient aligns better with the equilibrium orientation  $\alpha$ . A stronger cascade is observed in simulation LARGE than in simulation SMALL during this phase because of the lesser influence of diffusion effects. We have checked that the duration of this transient phase scales with the diffusive cascade time scale for both simulations.

Thereafter, in the final evolutionary stage of turbulence, both tracer gradients tend to align with each other and this effect is most pronounced for the strongest gradients. This result implies that both tracer cascades are similar in the final evolutionary stage of turbulence. This is corroborated both by the overlap of their spectra at small scales, and by identical alignments of their gradients with the equilibrium orientations mentioned above. These observations could result from the combined effects of advective dynamics (straining process) and diffusion effects which spatially align tracer gradients with the direction of the largest gradients.<sup>18</sup> It should be noted that the above results on the production of tracer gradients mostly concern small spatial scales, while passive and active tracers behave quite differently at intermediate and large scales of motion. Indeed, there is an accumulation of vorticity at large scales which is absent for the passive tracer case.

The effect of diffusion has been checked to play a preponderant role in the dynamics at time  $t \sim \tau_{\text{diff}}$  estimated in the present paper. As predicted by Constantin *et al.*,<sup>18</sup> diffusion has been found to have two effects. The first is to act as a classical diffusion term by suppressing spatial inhomogeneities. This reduces both the alignment of tracer gradients with the equilibrium orientations predicted for inviscid flow topology and the alignment of passive and active tracer gradients with each other. The second effect is to spatially align the tracer gradients in the direction of the largest gradients, while its quantitative influence on the latter is negligible.

A large part of this study has concerned the characterization of alignment properties, and we have distinguished the alignment of passive and active tracers with flow topology from their relative orientation. It should be emphasized that the latter is the most pronounced quantitatively and this holds for both short times (when  $t \sim \tau_{\text{adv}} \ll \tau_{\text{diff}}$ ) and for long times ( $t \gg \tau_{\text{diff}}$ ). So a common nature of the dynamics of passive and active scalars can be expected and the equilibrium orientations determined by Lapeyre *et al.*<sup>8</sup> and Klein *et al.*<sup>9</sup> are only equilibrium estimates of the orientations determined by the flow topology. The differences and similarities of alignment between vorticity and passive scalar gradients can be explained by the structures present in the field. In physical space, the efficiency of the direct enstrophy cascade depends on the geometrical structures of the flow field: the direct cascade produces strong gradients which have a filamentary structure (with many strong vorticity gradients) while the inverse cascade produces closed streamlines (with relatively few vorticity gradients). The conjugation relationship between strain and vorticity creates differences between the tracer gradient dynamics and halts the direct cascade whenever structures with closed streamlines are present. On the other hand, at the spatial scales for which the enstrophy cascade is the most effective, the conjugation relationship is not efficient and both tracer gradients have identical dynamics. This explains why the differences between both tracer gradients vanish for the strongest gradients.

## ACKNOWLEDGMENTS

Computing resources were provided by Institut du Développement et des Ressources en Informatique Scientifique (France). We thank Armando Babiano for his suggestions on the effects of diffusion and Claude Basdevant for suggesting simulation LARGE.

- <sup>1</sup>G. Holloway and S. S. Kristmannsson, "Stirring and transport of tracer fields by geostrophic turbulence," *J. Fluid Mech.* **141**, 27 (1984).
- <sup>2</sup>A. Babiano, C. Basdevant, B. Legras, and R. Sadourmy, "Vorticity and passive-scalar dynamics in two-dimensional turbulence," *J. Fluid Mech.* **183**, 379 (1987).
- <sup>3</sup>K. Ohkitani, "Wave number space dynamics of enstrophy cascade in a forced two-dimensional turbulence," *Phys. Fluids A* **3**, 1598 (1991).
- <sup>4</sup>A. Okubo, "Horizontal dispersion of floatable particles in the vicinity of velocity singularity such as convergences," *Deep-Sea Res.* **17**, 445 (1970).
- <sup>5</sup>J. Weiss, "The dynamics of enstrophy transfer in two-dimensional hydrodynamics," *Physica D* **48**, 273 (1991).
- <sup>6</sup>B. Protas, A. Babiano, and N. K.-R. Kevlahan, "On geometrical alignment properties of two-dimensional forced turbulence," *Physica D* **128**, 169 (1999).
- <sup>7</sup>B. L. Hua and P. Klein, "An exact criterion for the stirring properties of nearly two-dimensional turbulence," *Physica D* **113**, 98 (1998).
- <sup>8</sup>G. Lapeyre, P. Klein, and B. L. Hua, "Does the tracer gradient vector align with the strain eigenvectors in 2-D turbulence?" *Phys. Fluids* **11**, 3729 (1999).
- <sup>9</sup>P. Klein, B. L. Hua, and G. Lapeyre, "Alignment of tracer gradients in two-dimensional turbulence using second order Lagrangian dynamics," *Physica D* **146**, 246 (2000).
- <sup>10</sup>B. L. Hua, J. C. McWilliams, and P. Klein, "Lagrangian accelerations in geostrophic turbulence," *J. Fluid Mech.* **366**, 87 (1998).
- <sup>11</sup>K. Ohkitani, "Kinematics of vorticity: Vorticity-strain conjugation in incompressible fluid flows," *Phys. Rev. E* **50**, 5107 (1994).
- <sup>12</sup>K. Ohkitani, "Stretching of vorticity and passive vectors in isotropic turbulence," *J. Phys. Soc. Jpn.* **67**, 3668 (1998).
- <sup>13</sup>L. Rayleigh, "On the stability, or instability, of certain fluid motions," *Proc. London Math. Soc.* **11**, 57 (1880).
- <sup>14</sup>J. C. McWilliams, "A demonstration of the suppression of turbulent cascade by coherent vortices in two-dimensional turbulence," *Phys. Fluids A* **2**, 547 (1990).
- <sup>15</sup>D. G. Dritschel, P. H. Haynes, M. N. Jukes, and T. G. Shepherd, "The stability of a two-dimensional vorticity filament under uniform strain," *J. Fluid Mech.* **230**, 647 (1991).
- <sup>16</sup>N. K.-R. Kevlahan and M. Farge, "Vorticity filaments in two-dimensional turbulence: Creation, stability and effect," *J. Fluid Mech.* **346**, 49 (1997).
- <sup>17</sup>C. Basdevant and T. Philipovitch, "On the validity of the 'Weiss criterion' in two-dimensional turbulence," *Physica D* **73**, 17 (1994).
- <sup>18</sup>P. Constantin, I. Procaccia, and D. Segel, "Creation and dynamics of vortex tubes in three-dimensional turbulence," *Phys. Rev. E* **51**, 3207 (1995).
- <sup>19</sup>B. L. Hua and D. B. Haidvogel, "Numerical simulations of the vertical structure of quasigeostrophic turbulence," *J. Atmos. Sci.* **23**, 2923 (1986).
- <sup>20</sup>P. Santangelo, R. Benzi, and B. Legras, "The generation of vortices in high-resolution, two-dimensional decaying turbulence and the influence of initial conditions on the breaking of self-similarity," *Phys. Fluids A* **1**, 1027 (1989).
- <sup>21</sup>L. Shtilman, M. Spector, and A. Tsinober, "On some kinematic versus dynamic properties of homogeneous turbulence," *J. Fluid Mech.* **247**, 65 (1993).
- <sup>22</sup>J. C. McWilliams, "The emergence of isolated coherent vortices in turbulent flow," *J. Fluid Mech.* **146**, 21 (1984).
- <sup>23</sup>M. E. Brachet, M. Meneguzzi, H. Politano, and P. L. Sulem, "The dynamics of freely decaying two-dimensional turbulence," *J. Fluid Mech.* **194**, 333 (1988).